Journal of
Materials Chemistry C

Accepted Manuscript

Volume 4 | Number 1 | 7 January 2016 | Pages 1–224

Journal of
Materials Chemistry C

Materials for optical, magnetic and electronic devices
www.rsc.org/MaterialsC

ISSN 2050-7526

ROYAL SOCIETY
OF CHEMISTRY

PAPER
Nguyễn T. K. Thanh, Xiaodi Su et al.
Fine-tuning of gold nanorod dimensions and plasmonic properties using
the Hofmeister effects

175 YEARS

This is an Accepted Manuscript, which has been through the Royal Society of Chemistry peer review process and has been accepted for publication.

Accepted Manuscripts are published online shortly after acceptance, before technical editing, formatting and proof reading. Using this free service, authors can make their results available to the community, in citable form, before we publish the edited article. We will replace this Accepted Manuscript with the edited and formatted Advance Article as soon as it is available.

You can find more information about Accepted Manuscripts in the author guidelines.

Please note that technical editing may introduce minor changes to the text and/or graphics, which may alter content. The journal's standard Terms & Conditions and the ethical guidelines, outlined in our author and reviewer resource centre, still apply. In no event shall the Royal Society of Chemistry be held responsible for any errors or omissions in this Accepted Manuscript or any consequences arising from the use of any information it contains.

ROYAL SOCIETY
OF CHEMISTRY

rsc.li/materials-c

[60]PCBM Single Crystals: Remarkably Enhanced Band-like Charge Transport, Broadband UV-Visible-NIR Photo-responsivity and Improved Long-term Air-stability

Xiaoming Zhao,[1‡] Tianjun Liu,[2‡] Xueyan Hou,[1] Zilu Liu,[3] Wenda Shi,[1]* and T. John S. Dennis[1]*

[1] School of Physics and Astronomy and Materials Research Institute, Queen Mary University of London, Mile End Road, London E1 4NS, United Kingdom
[2] School of Engineering and Materials Science and Materials Research Institute, Queen Mary University of London, Mile End Road, London E1 4NS, United Kingdom
[3] School of Biological and Chemical Sciences and Materials Research Institute, Queen Mary University of London, Mile End Road, London E1 4NS, United Kingdom

* Corresponding author: Wenda Shi (email: w.shi@qmul.ac.uk) and T. John S. Dennis (email: j.dennis@qmul.ac.uk)

KEYWORDS: PCBM; Single crystal; Band-like charge transport; Photodetector

ABSTRACT: We report the charge transport mechanism, long-term stability and UV-Visible-NIR photo-responsivity of single crystals of [60]PCBM (phenyl-C_{61}-butyric acid methyl ester) – the dominant acceptor material in organic photovoltaics. Despite [60]PCBM's paramount role in such device, its intrinsic properties was largely unknown because of highly disordered solution-processed films, the electron transport mechanism remained ill-defined, and the long-term stability was poor – posing a major bottleneck for advancing cell efficiency and

stability. We employed a liquid−liquid interfacial precipitation strategy to grow single crystals of [60]PCBM, which allowed us to experimentally elucidate its electron transport properties, long-term stability and photo-responsivity. Temperature-dependent mobility studies enabled us to reveal its charge transport mechanism. Promisingly, [60]PCBM single crystals were found to exhibit a more favorable band-like charge transport mechanism at room temperature and present electron mobility exceeding their thin-film counterparts by two orders of magnitude. Photodetectors based on single crystals show broadband photo-responsivity from UV, Visible to NIR regions. Long-term stability test showed the performance of devices based on single crystals remained 80% after 480-hour aging, whereas the performance of thin film devices dropped by over 80% under the same condition. Our findings underscore single crystals as a key strategy to achieve breakthroughs in highly efficient and stable devices.

In recent years, organic semiconducting materials have attracted considerable interest because of their advantages of large-area coverage, low-cost processing, and structural flexibility.[1–5] The fullerene derivative of [6,6]-phenyl C61 butyric acid methyl ester ([60]PCBM) is an n-type organic semiconductor with good electric properties and solubility in most organic solvents.[6,7] These advantages allow tremendous applications of [60]PCBM in solution-processed organic field-effect transistors (OFETs), photodetectors (PDTs) and organic photovoltaics (OPVs).[8–12] Particularly, as the most widely used electron acceptor, [60]PCBM has important functions in OPVs with high power conversion efficiency.[13–15] However, most of

2

these applications are yet based on [60]PCBM in amorphous phase, which limits the enhancement of the device performance. Grain boundaries and molecular disorder in amorphous thin films scatter the charge carriers by the effect of coulomb scattering, which results in the reduction of charge carrier mobility.[16,17] The absence of these scattering centers is the fundamental merit of organic crystals.[18] A significant number of studies have considered that organic crystals are ideal materials for the enhancement in device performance because of their highly ordered molecules.[19–21] However, the side group attached to C_{60} makes [60]PCBM hard to crystallize, leading to the formation of disordered aggregates composed of nanocrystals rather than crystals in the microscopic scale, which has prevented the material from reaching its ultimate performance limits.[22,23] Thus, this challenge remains a major bottleneck in the advancement of device performance. Particularly in the case of OPVs, tremendous efforts have been made to design and synthesize new organic electron conductors as "fullerene-free" electron acceptor alternatives.[24,25]

Thus, we were motivated to grow single crystals of [60]PCBM to address the lack of fundamental understanding of its intrinsic stability, photo-responsivity and charge transport properties, particularly their intrinsic upper limit of electron mobility, and to reveal a clear mechanism for charge transport that could be used to devise rational strategies for engineering this crucial device component.[26]
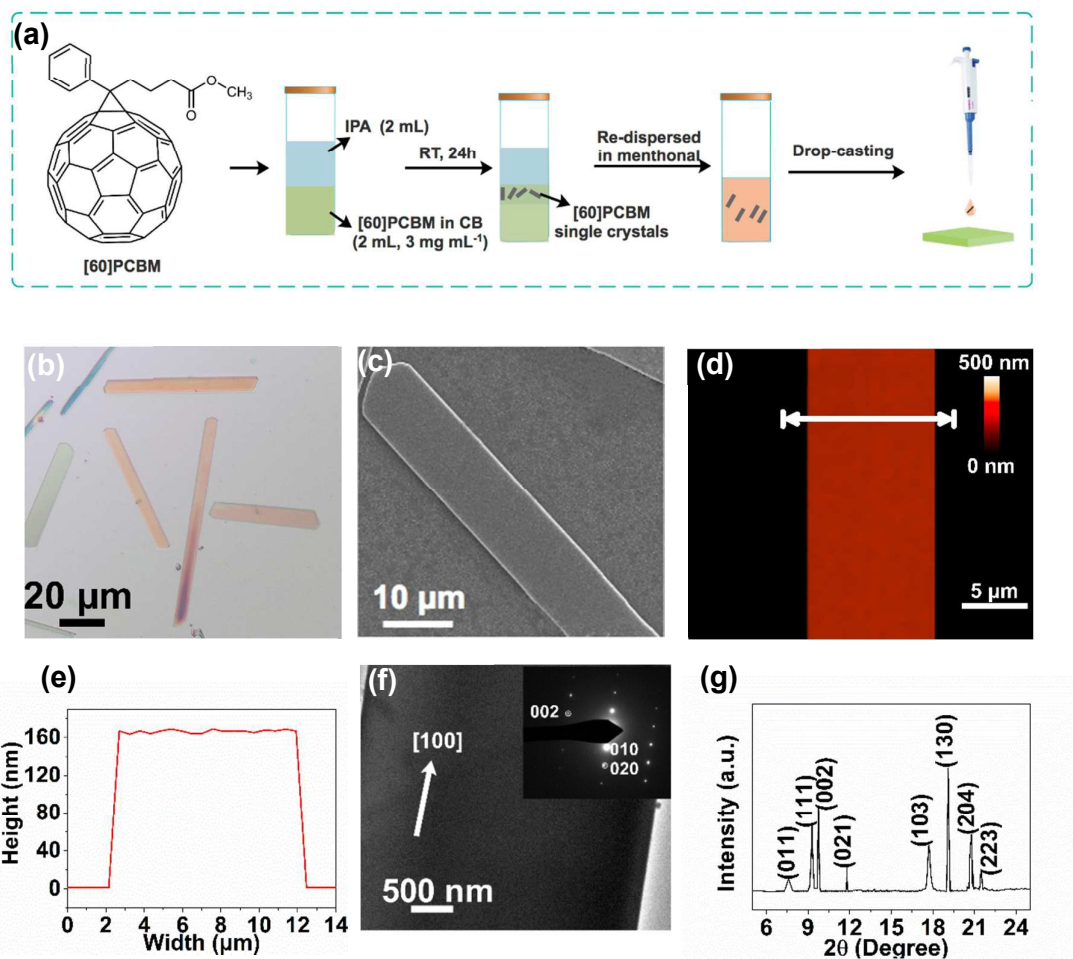
Figure 1 (a) Schematic diagram of [60]PCBM single crystals growth by liquid−liquid interfacial precipitation method; (b) OM image, (c) SEM image and (d) AFM 2D image with (e) corresponding height profile of [60]PCBM single crystals; (f) TEM image and (inset) corresponding SAED pattern and (g) XRD pattern of [60]PCBM single crystals.

Single Crystal Growth and Characterization

[60]PCBM ribbon-like single crystals were obtained through liquid−liquid interfacial precipitation method,[23] as shown in **Figure 1a**. After [60]PCBM is dissolved in chlorobenzene (CB) at a concentration of 3 mg mL^{-1}, the antisolvent isopropanol (IPA) was injected onto the surface of [60]PCBM solution. Thus, a liquid−liquid interface is formed. The diffusion of the antisolvent into PCBM solution will drive the precipitation of [60]PCBM in the form of crystals. After 24 hours' growth, [60]PCBM single crystals are achieved. The crystals obtained were then re-dispersed in tiny amount of methanol, producing a suspension well-suited for moving onto a substrate by pipette. After 24 hours' thermal annealing under vacuum to remove the residual solvent molecules,[27] the samples can be used for microscopy imaging or device fabrication.

After obtaining [60]PCBM single crystals, we proceed to characterize their morphologies *via* optical microscope (OM), scanning electron microscopy (SEM) and atomic force microscopy (AFM), as shown in **Figure 2b-e**, respectively. The OM images (**Figure 1b**) show that the [60]PCBM ribbon crystals exhibit micrometer-scale length. 50 individual crystals were studied and the histogram of their dimensions are summarized in **Figure S1**. The average lengths achieved on 50 individual crystals is (138 ± 28.6) μm. [60]PCBM ribbon crystals present two-dimensional nano-structures with the width of (13.4 ± 3.15) μm and the thickness of (148 ± 34.8) nm. The crystal structures of [60]PCBM ribbon crystals were studied by select area electron

diffraction (SAED) as shown in **Figure 1f**. The presence of discrete diffraction points, and the fact that no change in the SAED patterns is observed for different parts of the same single crystals, indicates the single crystallinity of [60]PCBM ribbon crystals. To further confirm the crystal structure, we performed an X-ray diffraction (XRD) study. The room-temperature XRD pattern of the as-prepared single crystals is shown in **Figure 1g**. The structure can be indexed with a solvent-free monoclinic crystal system with cell dimensions of a = 13.34 Å, b = 15.57 Å, c = 19.47 Å, which well coincides with the previous report in the literature.[27] These morphology studies indicate that high quality [60]PCBM single crystals are successfully obtained.
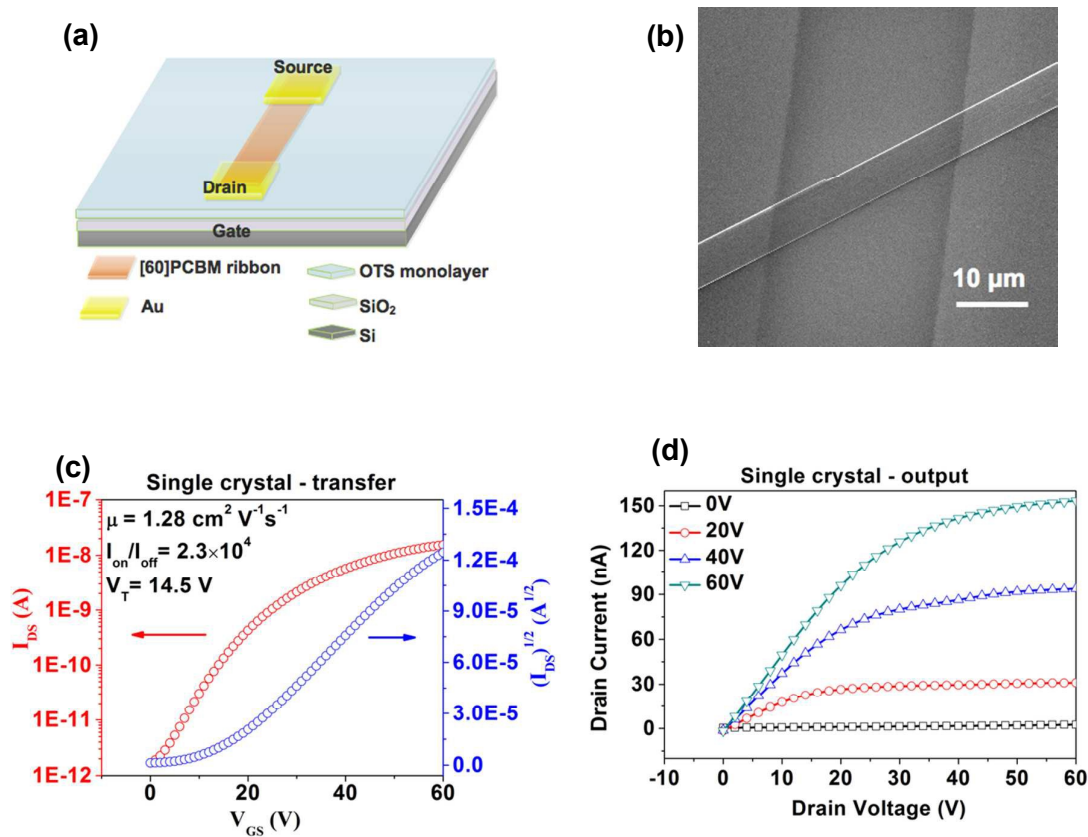
Figure 2 (a) Schematic diagram and (b) SEM image of device structure based on [60]PCBM single crystals; (c) Typical transfer characteristics of single crystal devices in n-channel operation mode under positive drain bias; (d) Typical output characteristics of single crystal device in n-channel operation mode under positive drain bias.

Charge Transport Properties

The single-crystalline nature of [60]PCBM ribbons indicates their potential use in studying the intrinsic charge transport properties. This is because the minimized molecular disorder and defects usually give organic single crystal a high charge mobility, which is required in organic electronic device, such as OFETs and PDTs, to reduce the recombination of charge carriers.[28–30] Different methods have been used to assess the carrier mobility in organic materials like time-of-flight (TOF) methods, space charge limited current (SCLC) methods and organic field-effect transistor (OFET) methods. Among them, the OFET method is most frequently used due to its ability to combine a rather simple and flexible implementation with accurate and reproducible results.[31] Therefore, in this work we employed this method to study the charge transport properties of [60]PCBM single crystals.

OFET devices based on single crystals were fabricated with bottom-gate and top-contact configuration. **Figures 2a and b** respectively show the schematic diagram and the SEM images of the single crystal OFET device. Typical transfer characteristics of single crystal device is shown in **Figure 2c**. The output characteristics in n-channel operation modes is shown in **Figure 2d**, indicating excellent gate modulation. The mobility was gate bias dependent and we extracted the mobility by linear fitting of $(I_{DS})^{1/2}$ vs V_{GS} curves. The best charge transport performance achieved from single crystal devices was an electron mobility (μ_e) of 1.28 cm^2 V^{-1} s^{-1} as shown in **Figure 2c**. The histograms of electron mobility obtained from 50 devices are shown in **Figure S2**. We achieved an average μ_e of (0.98 ± 0.18)

cm^2 V^{-1} s^{-1} (range: 0.65 – 1.28), I_{on}/I_{off} > 10^4, and V_T between 11.3 and 15.3 V. OFETs based on [60]PCBM thin films were also fabricated for comparison. The fabrication details were included in **Experimental Section** and the OM and AFM images of device structure were shown in **Figure S3 and S4** in the Supporting Information. For thin film devices, the best charge transport performance achieved was a relatively low μ_e of 6.9 × 10^{-3} cm^2 V^{-1} s^{-1} as shown in **Figure S5**. The output characteristics in n-channel operation modes of thin-film devices is shown in **Figure S6**, indicating excellent gate modulation. With 50 devices tested, average μ_e of (4.6 ± 1.4 × 10^{-3}) cm^2 V^{-1} s^{-1} (range: 2.1 – 6.9×10^{-3}, **Figure S7**), I_{on}/I_{off} > 10^2, and V_T between 23.5 and 36.3 V were obtained.

This comparison clearly indicates the much better charge transport properties of [60]PCBM single crystals; as they exhibit an electron mobility more than two orders magnitude higher than that of the thin-film counterparts. This excellent feature will benefit both OPV and PDT devices. For OPVs, higher charge mobility is attribute to reduction of the charge carrier recombination to enhance the performance of organic photovoltaics,[28–30] while for PDTs, higher charge mobility would lead to high efficiency of the extraction of photo-generated carriers, and result in the better performance of PDTs.[32]
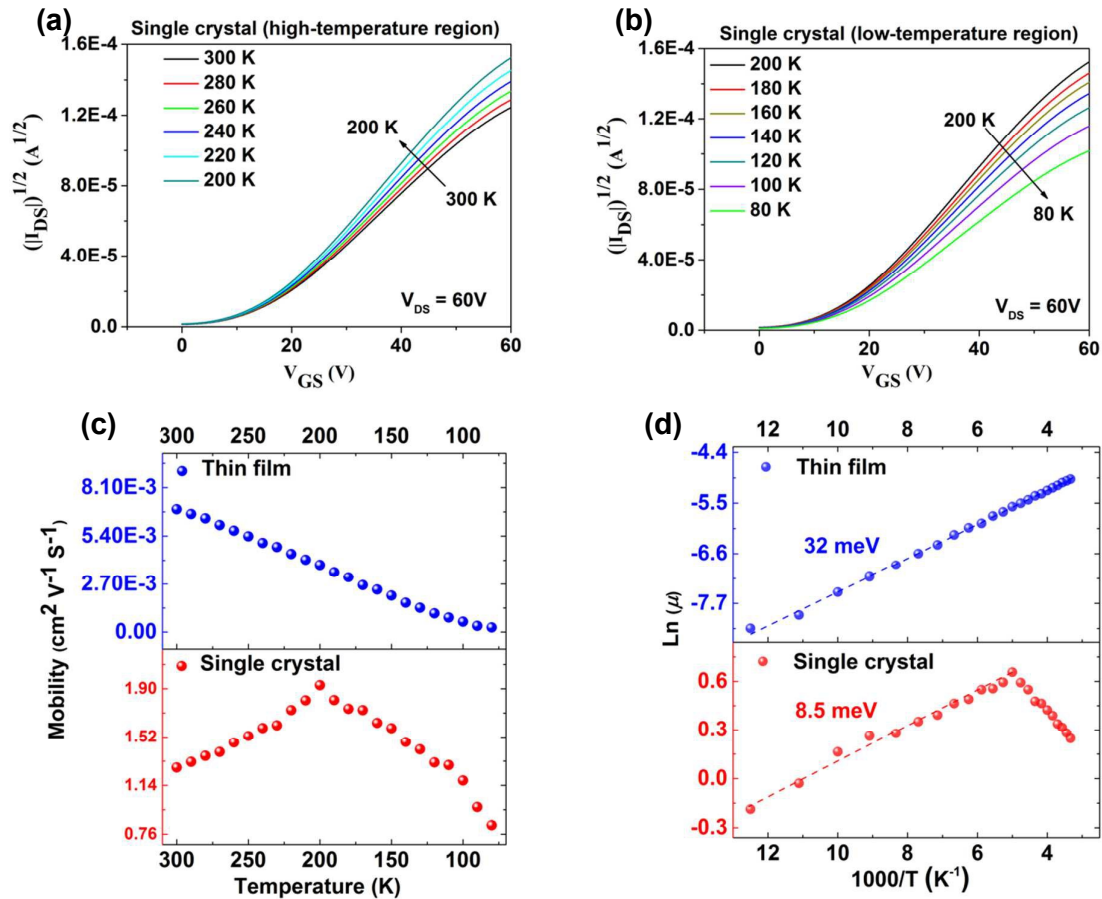
Figure 3 Transfer characteristics of single crystal devices in n-channel operation mode at the temperature from (a) 300K to 200K and (b) 200K to 80K; (c) Temperature dependence of mobility and (d) Ln(μ) versus $1/T$ for these two kinds of devices.

Band-like Charge Transport Mechanism

To study the charge transport mechanism in [60]PCBM single crystals, temperature-dependent mobility were tested in a vacuum holder by cooling samples from 300 to 80 K. The electron mobilities were measured every 10 K. **Figure 3a, b** and **Figure S8, S9** respectively show the OFET transfer curves of single crystals and thin films at the temperature from 300 K to 80 K with the square root of drain current plotted against the gate voltage. Interestingly, as shown in the **Figure 3c**, the electron mobility in [60]PCBM single crystals exhibit an increase-at-first-and-then-decrease behavior by cooling the samples while for [60]PCBM thin films, the electron mobility decrease monotonically with lower temperature. In the low-temperature region (80 K – 200 K, **Figure 3b and S9**), the electron mobility of both single crystals and thin films decreased by cooling the samples, yielding a positive mobility temperature coefficient ($d\mu/dT > 0$). Such behavior is commonly observed in organic field effect transistors,[33–36] reflecting the gate voltage filling up low-mobility trap states.[37] This implies that a thermally activated mechanism governs the electron transport in [60]PCBM single crystals and thin films at low temperature regions. In low temperature regions, most charge carriers are trapped in localized shallow traps formed by chemical impurities, sites of structural disorder, and surface states, and then charge transport occurs through extended states (transport level) when the carriers are thermally activated (released) from the traps. Fitting the data with the equation (1),[38]

$$\mu = \mu_0 \exp\left(\frac{-E_a}{k_B T}\right) \qquad (1)$$

11

where E_a is the activation energy and k_B is the Boltzmann constant, leads to activation energies of 8.5 meV for single crystals and 32 meV for thin films, as shown in **Figure 3d**. The activation energy of single crystals here is much lower than that of thin film, suggesting a much lower degree of disorders presented in the single crystals and at the interface between the semiconductors and the substrates than thin films.

On the other hand, in the high-temperature region, the electron mobility of single crystals increases monotonically upon cooling the samples from 300 to 200 K, exhibiting a negative mobility temperature coefficient ($d\mu/dT < 0$). The observation of the negative mobility temperature coefficients is a general signature of charge carrier delocalization over a few molecules, which is the band-like charge transport.[38,39] In the high-temperature region, sufficient thermal energy is available such that the influence of trapping could be eliminated and the overall conduction was determined by the intrinsic transport through the extended transport level within the single crystals. Band-like temperature dependence is the signature of high-quality crystals and excellent electrical conduction.[33] For thin-film counterparts, like the low-temperature region, the electron mobility decrease monotonically by cooling the samples at the high temperature region, without favorable band-like charge transport mechanism.

The relatively high electron mobility, highly-efficient band-like charge transport at room temperature, together with the excellent electrical conduction, makes [60]PCBM single crystals a promising replacement of the thin-film counterparts with

the potential ability to generate higher-density photocurrent for OPVs and highly efficient extraction of photo-generated carriers for PDTs.
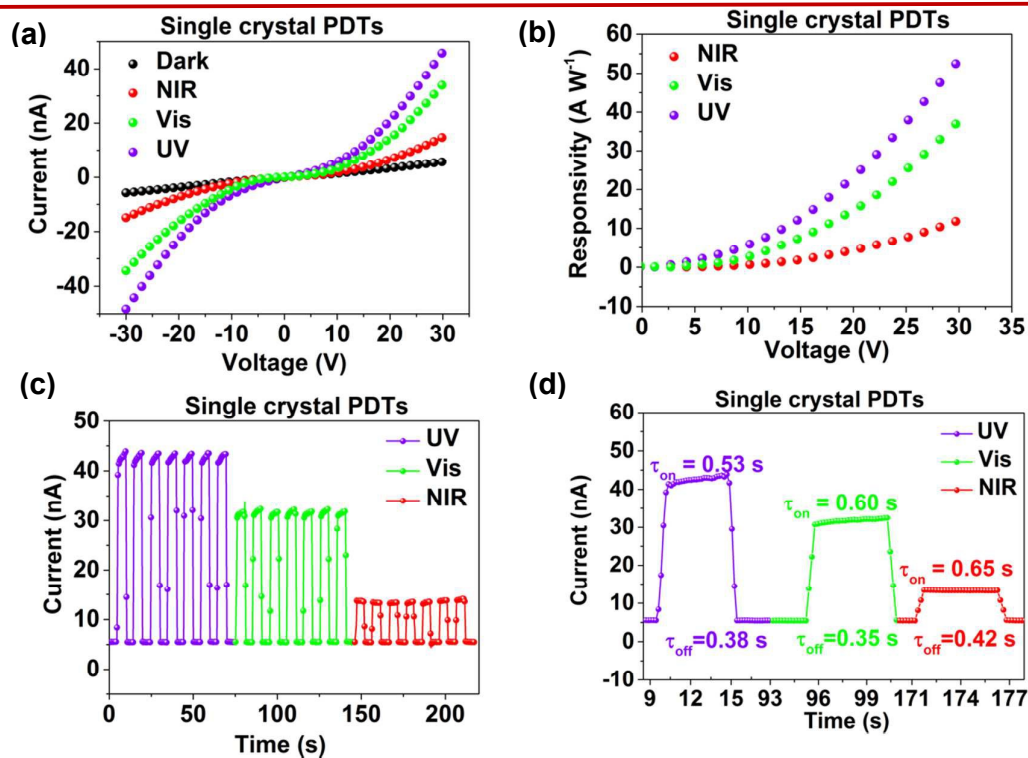

Figure 4 Photo-response characteristics of [60]PCBM single crystal devices. (a) I−V curves, (b) responsivity, (c) time-resolved photocurrent response and (d) enlarged portions of one response and reset process illuminated by UV, Vis and NIR lasers.

13

Photo-responsivity

To compare the practical applications of [60]PCBM single crystals and thin films, we fabricated organic photodetectors (PDTs) based on both single crystals, and thin films. Two kinds of device were fabricated on silicon substrates with a thermal oxide layer that was 300 nm thick. For comparison reasons, both devices were made with identical channel lengths of 20 μm. The electrical properties were measured using a traditional two terminal method.[40] Photo-response characteristics under UV (350 nm), visible (550 nm) and NIR (780 nm) laser diodes with the power intensity of 5 mW cm^{-2} are shown in **Figure 4a-d** for single crystal device and **Figure S10-S13** for the thin film device.

Figure 4a and S10 shows typical current *versus* voltage curves of single crystals and thin film photodetectors in the dark and under laser illumination. The slight nonlinearity of the $I-V$ curves results from the work-function mismatch between semiconductors and the gold contacts used in out devices. A drastic increase in current under laser illumination is observed when compared to the current in the dark.

Photoresponsivity, R, is a key factor to identify the light-sensitive performance of photodetectors. To further evaluate the photo-response, we calculated photo-responsivity of single crystal and thin film devices by the Equation (2):[41]

$$R = \frac{I_{light} - I_{dark}}{PS} \qquad (2)$$

Where I_{light} is the current when exposed to laser illumination, I_{dark} is the dark current, P is the incident power density and S is the effective illuminated area. The effective irradiated areas are approximately 151.3 and 1361.3 μm^2 for single crystal

14

and thin films devices, respectively. The single crystal photodetector clearly has a substantially higher performance than the thin film device. As depicted in **Figure 4b and S11**, at an applied bias of 30 V, under UV, visible and NIR laser illumination, single crystal devices achieve responsivities of 52.6, 36.9 and 11.8 A W^{-1} respectively. These values are over one order magnitude higher than the responsivities (3.52, 1.56 and 1.03 A W^{-1} under UV, visible and NIR illumination respectively) of the thin film devices under the same condition. It has been reported that the charge mobility of channels had a drastic influence on the sensitivity of photodetectors: whereby channels with higher charge mobility would yield higher responsivity.[32] In our case, [60]PCBM single crystals ($\sim$0.98 cm^2 V^{-1} s^{-1}) has a much higher mobility than its thin film counterparts ($\sim$4.6 $\times$ 10^{-3} cm^2 V^{-1} s^{-1}), which leads to high efficiency of the extraction of photo-generated carriers, and result in the better performance of single crystals than thin films in PDTs.

Figure 4c and S12 displays the time-resolved current response of both photodetectors with the laser switched on and off at a fixed voltage of 30 V. Under illumination of same wavelength, the "on" and "off" states keep the same current level for several cycles for single crystals devices, indicating the excellent reversibility and stability of single crystal photodetectors, while thin film devices show poor reversibility. Furthermore, analysis of an enlarged photo-response process containing one rise and one reset (**Figure 4d and S13**) shows both the rising and reset time of the single crystal devices are faster than those of the thin film devices. It is worth noting that [60]PCBM single crystals have photo-response at NIR region,

although the photo responsivity is relatively lower (11.8 A W^{-1}) to those in UV and visible region. It is reported by Curry *et al.* that fullerene single crystal has a unique extended absorption in NIR region compared to its thin film counterparts.[42] To confirmed this in [60]PCBM single crystals, we performed UV-Vis absorption measurements of [60]PCBM single crystals and thin films, and the spectrum is shown in **Figure S14**. It clearly shows that in the NIR region, [60]PCBM single crystals have more intensive absorption than its thin films, which leads to the higher NIR photo responsivity of [60]PCBM single crystals than thin films.

The better reversibility, faster detection time and the higher responsivity of single crystal devices further demonstrate the excellence of [60]PCBM single crystals than thin films for practical applications.
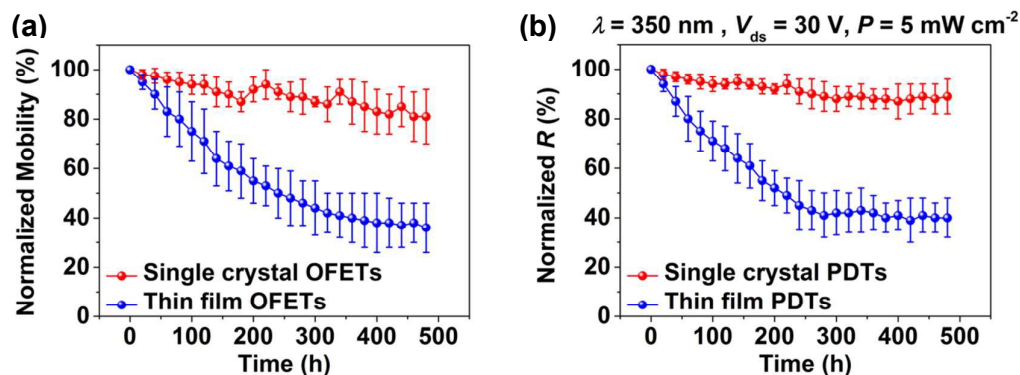
Figure 5 (a) Normalized electron mobility of the single crystal OFETs and thin film OFETs in ambient environment without encapsulation as a function of storage time. (b) Normalized responsivity of the single crystal photodetectors and thin film photodetectors in ambient environment without encapsulation as a function of storage time. The temperature and relative humidity is 23 ℃ and 30%.

Long-term Stability

One crucial factor for the suitable use of OFETs, PDTs and OPVs is the stability of these devices under ambient conditions. It was reported single crystals showed better moisture stability than the polycrystalline thin films due to the absence of grain boundaries.[43,44] Therefore, the air stability of the single crystal devices should be better than that of polycrystalline thin-film devices. To confirm this, we evaluate the long-term stability of the single crystal devices the and thin film devices in air. As shown in **Figure 5a and b**, the performance of single crystal devices remains almost 80% after the device was stored in air for 20 days, which is much better than the thin-film devices, which lost about 80% of their performance under the same condition.

In summary, the charge transport properties, photo-responsivity and long-term stability of [60]PCBM single crystals have been demonstrated. Compared to thin film counterparts, [60]PCBM single crystal exhibits higher electron mobility with band-like charge transport property at room temperature. In addition, [60]PCBM single crystal present more promising broadband UV-visible-NIR photo-response and much better long-term device stability. Our work here not only elucidates a straightforward and assured strategy for creating a vastly improved n-type semiconductor through improving the crystallinity of [60]PCBM, one of the most widely used commercially available n-type semiconductors for photovoltaic and optoelectronic devices, but also highlights mesoscale molecular ordering as the key to promoting the material's charge transport properties, and thus enhance the device performance accordingly. Our work clearly show the great enhancement by employing [60]PCBM single crystals in OFETs and PDTs. For organic photovoltaics, the relevant work is in progress.

Methods

Materials: [60]PCBM with purity of 99.95% was purchased from Ossila. n-Octadecyltrimethoxysilane (OTS) was purchased from Sigma Aldrich. CB, IPA and other solvents were purchased from Sigma Aldrich. All materials were used without further purification.

Wafer modification: Highly doped silicon substrates (1 cm^2) with 300 nm SiO$_2$ were used for FET substrates. Before crystallization, the wafers were modified by OTS monolayer following previous report.[45]

Crystallization: [60]PCBM ribbon crystals were grown by liquid−liquid interfacial precipitation method referring to the literature.[23] Firstly, [60]PCBM was dissolved in CB (3 mg mL^{-1}) with the assistance of ultrasonic oscillating for 25 min. 2 mL of the resulting solutions were injected into the 10 mL bottle. Then, IPA of 2 mL was slowly added into the bottles along the wall. This system was kept still until the precipitation of [60]PCBM crystals. The precipitated crystals were filtered with a 220 μm filter and re-dispersed in tiny amount of methanol, producing a suspension well-suited for deposition on a substrate either for microscopy imaging or device fabrication. The single crystals were deposited on the substrate and then the substrate was placed in a holder under a vacuum of 10^{-6} Torr for 24 h to remove the remaining solvent.

Morphology Characterization and Crystallography: OM images were recorded using an Leica, DM4000 optical microscope. A NT-MDT Ntegra atomic force microscope in semi-contact mode was used to characterize surface morphology of the single crystals. SEM images were recorded by an FEI Inspect-F scanning electron

Journal of Materials Chemistry C Accepted Manuscript

microscope. TEM observations were performed with an SAED configuration on a

JEOL JEM-2010 transmission electron microscope with an accelerating voltage of

200 kV. XRD pattern was obtained by a Rigaku D/max-2500 X-ray diffractometer

using filtered Cu Kα radiation (λ = 1.54 Å).

OFET fabrication and characterization: OFETs were constructed in a bottom-gated

configuration by depositing top-contact source and drain electrodes (50 nm Au), with

channel lengths (L) of 20 μm for both thin film and single crystal OFETs and the

channel width (W) of single crystal devices was measured from the contacting area of

the crystals that cross the S and D electrodes. To deposit [60]PCBM thin film

channels, 10 mg mL^{-1} [60]PCBM was dissolved in chlorobenzene. The as-prapared

solution was spin-coated on substrates at 2500 rmp for 30 s. Current–voltage

characteristics of the devices were measured under ambient conditions on a Lake

Shore model PS-100 tabletop cryogenic probe tation with a Keithley 4200-SCS

semiconductor parameter analyzer. The measured capacitance of the OTS-modified

SiO$_2$/Si substrates was 11 nF cm^{-2}. The field-effect mobility was calculated in the

saturation regime by using the equation $I_{DS} = (\mu W C_i / 2L)(V_G - V_T)^2$, where I_{DS} is the

drain–source current, μ is the field-effect mobility, W is the channel width, L is the

channel length, C_i is the capacitance per unit area of the gate dielectric layer, V_G is the

gate voltage and V_T is the threshold voltage.

Electrical Measurement at Varied Temperatures: The current-voltage measurement

was carried out on the same Lake Shore model PS-100 tabletop cryogenic probe

station at a background pressure of 1×10^{-6} torr or lower. The controlled cooling from

300 K to 80 K was realized by introducing liquid nitrogen into the insulation cabin outside the sample cabin. Temperature of the samples was balanced by simultaneous heating with a hot plate under the sample holder.

Photodetector Fabrication and Photoresponse Measurement: Photodetectors were fabricated by dispersing single crystals on silicon wafers with a 300 nm thick thermal oxide layer. The electrical contacts to individual single crystals were defined by copper grid shadow mask with the typical gap of 20 μm, and subsequently 50 nm Au was evaporated. Photoresponse measurements were performed on the same Lake Shore model PS-100 tabletop cryogenic probe tation by two-terminal mode with an applied bias of 30 V. The devices were tested under ambient conditions. The parameters were analyzed using a Keithley 4200-SCS semiconductor characterization system. 350 nm, 550 nm and 780 nm UV, visible and NIR laser diodes were used to illuminate the devices to initiate the photocurrent. UV-Vis absorption spectra were recorded by a Cary 60 UV-Vis spectrometer.

Data availability: The data that support the plots within this paper and other findings of this study are available from the corresponding author upon reasonable request.

ASSOCIATED CONTENT

Supporting Information.

Histogram of mobility calculated from 50 OFETs based on the [60]PCBM single crystals or the thin films.

AUTHOR INFORMATION

Corresponding Author

*Email: Wenda Shi (email: w.shi@qmul.ac.uk), T. John S. Dennis (email:

j.dennis@qmul.ac.uk).

‡Xiaoming Zhao and Tianjun Liu contributed equally.

Author Contributions

X.Z. conceived the idea and design of the experiments. X.Z. performed the single crystal growth of [60]PCBM. X.Z. and X.H. carried out the image collection and result analysis of OM. X.Z. and W.S. carried out the image collection and result analysis of SEM. X.Z. and Z.L. carried out the image collection and result analysis of AFM. X.Z. and T.L. performed the measurements and result analysis of XRD, TEM and SAED. X.Z. fabricated the OFET devices and performed the temperature-dependent measurements and data analysis. X.Z. fabricated the photodetectors and carried out the photo-response measurements and data analysis. X.Z. carried out the long-term stability of devices. X.Z. drafted the manuscript and all authors contributed to the revision of the manuscript. T.J.S.D. supervised this work.

Notes

The authors declare no competing financial interest.

ACKNOWLEDGMENT

**Journal of Materials Chemistry C Accepted Manuscript**

REFERENCES

1   X. Zhao, S. Wang, J. You, Y. Zhang and X. Li, *J. Mater. Chem. C*, 2015, **3**, 11377–11384.

2   P. Qi, F. Zhang, X. Zhao, X. Liu, X. Bi, P. Wei, Y. Xiao, X. Li and S. Wang, *Energy Technol.*, 2017, **5**, 1173–1178.

3   F. Zhang, X. Zhao, C. Yi, D. Bi, X. Bi, P. Wei, X. Liu, S. Wang, X. Li, S. M. Zakeeruddin and M. Grätzel, *Dye. Pigment.*, 2017, **136**, 273–277.

4   X. Zhao, F. Zhang, C. Yi, D. Bi, X. Bi, P. Wei, J. Luo, X. Liu, S. Wang, X. Li, S. M. Zakeeruddin and M. Grätzel, *J. Mater. Chem. A*, 2016, **4**, 16330–16334.

5   E. Menard, M. A. Meitl, Y. Sun, J. U. Park, D. J. L. Shir, Y. S. Nam, S. Jeon and J. A. Rogers, *Chem. Rev.*, 2007, **107**, 1117–1160.

6   W. Shi, X. Hou, T. Liu, X. Zhao, A. B. Sieval, J. C. Hummelen and T. J. S. Dennis, *Chem. Commun.*, 2017, **53**, 975–978.

7   F. Zhang, W. Shi, J. Luo, N. Pellet, C. Yi, X. Li, X. Zhao, T. J. S. Dennis, X. Li, S. Wang, Y. Xiao, S. M. Zakeeruddin, D. Bi and M. Grätzel, *Adv. Mater.*, 2017, **29**, 1606806.

8   W. Ma, C. Yang, X. Gong, K. Lee and a. J. Heeger, *Adv. Funct. Mater.*, 2005, **15**, 1617–1622.

9   S. Cho, J. H. Seo, K. Lee and A. J. Heeger, *Adv. Funct. Mater.*, 2009, **19**, 1459–1464.

10   B. C. Thompson and J. M. J. Fréchet, *Angew. Chemie - Int. Ed.*, 2008, **47**, 58–77.

11   Z. Liu, K. Parvez, R. Li, R. Dong, X. Feng and K. Müllen, *Adv. Mater.*, 2015,
        27, 669–675.

12   K. Szendrei, F. Cordella, M. V. Kovalenko, M. Böberl, G. Hesser, M. Yarema,
        D. Jarzab, O. V. Mikhnenko, A. Gocalinska, M. Saba, F. Quochi, A. Mura, G.
        Bongiovanni, P. W. M. Blom, W. Heiss and M. A. Loi, *Adv. Mater.*, 2009, **21**,
        683–687.

13   G. H. Jun, S. H. Jin, B. Lee, B. H. Kim, W.-S. Chae, S. H. Hong and S. Jeon,
        Energy Environ. Sci., 2013, **6**, 3000-3006.

14   P. Yang, D. F. Zeigler, K. C. Bryant, T. R. Martin, D. R. Gamelin and C. K.
        Luscombe, *J. Mater. Chem. C*, 2014, **2**, 4922–4927.

15   P. Kubis, L. Lucera, F. Machui, G. Spyropoulos, J. Cordero, A. Frey, J.
        Kaschta, M. M. Voigt, G. J. Matt, E. Zeira and C. J. Brabec, *Org. Electron.*
        physics, Mater. Appl., 2014, **15**, 2256–2263.

16   T. Hasegawa and J. Takeya, *Sci. Technol. Adv. Mater.*, 2009, **10**, 24314.

17   C. Reese and Z. Bao, *Mater. Today*, 2007, **10**, 20–27.

18   T. Hallam, M. Lee, N. N. Zhao, I. Nandhakumar, M. Kemerink, M. Heeney, I.
        McCulloch and H. Sirringhaus, *Phys. Rev. Lett.*, 2009, **103**, 1–4.

19   X. Zhao, T. Liu, Y. Cui, X. Hou, Z. Liu, X. Dai, J. Kong, W. Shi and T. J. S.
        Dennis, *Nanoscale*, 2018, DOI: 10.1039/C8NR01305E.

20   X. Zhao, T. Liu, W. Shi, X. Hou, Z. Liu and T. J. S. Dennis, *J. Phys. Chem. C*,
        2018, DOI: 10.1021/acs.jpcc.8b01845.

21   X. Zhao, T. Liu, Y. Zhang, S. Wang, X. Li, Y. Xiao, X. Hou, Z. Liu, W. Shi
      and T. J. S. Dennis, *Adv. Mater. Interfaces* 2018, DOI:
      10.1002/admi.201800336

22   Y. Yang, C. Liu, S. Gao, Y. Li, X. Wang, Y. Wang, T. Minari, Y. Xu, P.
      Wang, Y. Zhao, K. Tsukagoshi and Y. Shi, *Mater. Chem. Phys.*, 2014, **145**,
      327–333.

23   L. Zheng and Y. Han, *J. Phys. Chem. B*, 2012, **116**, 1598–1604.

24   N. Beaumont, S. W. Cho, P. Sullivan, D. Newby, K. E. Smith and T. S. Jones,
      Adv. Funct. Mater., 2012, **22**, 561–566.

25   H. Zhong, C. H. Wu, C. Z. Li, J. Carpenter, C. C. Chueh, J. Y. Chen, H. Ade
      and A. K. Y. Jen, *Adv. Mater.*, 2016, **28**, 951–958.

26   J. D. Servaites, M. A. Ratner and T. J. Marks, *Energy Environ. Sci.*, 2011, **4**,
      4410-4414.

27   G. Paternò, A. J. Warren, J. Spencer, G. Evans, V. G. Sakai, J. Blumberger and
      F. Cacialli, *J. Mater. Chem. C*, 2013, **1**, 5619-5623.

28   P. Vanlaeke, A. Swinnen, I. Haeldermans, G. Vanhoyland, T. Aernouts, D.
      Cheyns, C. Deibel, J. D'Haen, P. Heremans, J. Poortmans and J. V. Manca,
      Sol. Energy Mater. Sol. Cells, 2006, **90**, 2150–2158.

29   D. Chen, A. Nakahara, D. Wei, D. Nordlund and T. P. Russell, *Nano Lett.*,
      2011, **11**, 561–567.

30   H. Zhang, L. Jiang, Y. Zhen, J. Zhang, G. Han, X. Zhang, X. Fu, Y. Yi, W. Xu
      and H. Dong, *Adv. Electron. Mater.*, 2016, **2**, 1500423.

31   M. Morana, P. Koers, C. Waldauf, M. Koppe, D. Muehlbacher, P. Denk, M.

      Scharber, D. Waller and C. Brabec, *Adv. Funct. Mater.*, 2007, **17**, 3274–3283.

32   J. Wang, F. Liu, G. Wang, L. Wang and C. Jiang, *Org. Electron.*, 2016, **38**,

      158–163.

33   N. A. Minder, S. Ono, Z. Chen, A. Facchetti and A. F. Morpurgo, *Adv. Mater.*,

      2012, **24**, 503–508.

34   B. J. Kim, H. Yu, J. H. Oh, M. S. Kang and J. H. Cho, *J. Phys. Chem. C*, 2013,

      117, 10743–10749.

35   N. A. Minder, S. Lu, S. Fratini, S. Ciuchi, A. Facchetti and A. F. Morpurgo,

      Adv. Mater., 2014, **26**, 1254–1260.

36   Y. Krupskaya, M. Gibertini, N. Marzari and A. F. Morpurgo, *Adv. Mater.*,

      2015, **27**, 2453–2458.

37   X. Xu, Y. Yao, B. Shan, X. Gu, D. Liu, J. Liu, J. Xu, N. Zhao, W. Hu and Q.

      Miao, *Adv. Mater.*, 2016, **28**, 5276–5283.

38   T. Sakanoue and H. Sirringhaus, *Nat. Mater.*, 2010, **9**, 736–740.

39   C. Liu, T. Minari, X. Lu, A. Kumatani, K. Takimiya and K. Tsukagoshi, *Adv.

      Mater.*, 2011, **23**, 523–526.

40   Z. Wang, M. Safdar, C. Jiang and J. He, *Nano Lett.*, 2012, **12**, 4715–4721.

41   Y. Xie, M. Gong, T. A. Shastry, J. Lohrman, M. C. Hersam and S. Ren, *Adv.

      Mater.*, 2013, **25**, 3433–3437.

Journal of Materials Chemistry C Accepted Manuscript

42   Y. Jin, R. J. Curry, J. Sloan, R. a. Hatton, L. C. Chong, N. Blanchard, V.

Stolojan, H. W. Kroto and S. R. P. Silva, *J. Mater. Chem.*, 2006, **16**,

3715-3720.

43   Q. Dong, Y. Fang, Y. Shao, P. Mulligan, J. Qiu, L. Cao and J. Huang, *Science*,

2015, **347**, 967–970.

44   Y. Zhang, D. Li and C. Jiang, *Appl. Phys. Lett.*, 2013, **103**, 213304.

45   Y. Ito, A. A. Virkar, S. Mannsfeld, J. H. Oh, M. Toney, J. Locklin and Z. Bao,

J. Am. Chem. Soc., 2009, **131**, 9396–9404.
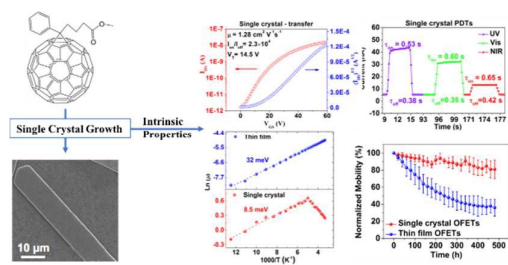
[60]PCBM single crystals were prepared to understand its intrinsic photo-responsivity, stability, and charge transport properties.